

lower threshold and the other CF had an increasingly higher threshold. The occurrence at regular depth intervals of transitions from single-peaked to double-peaked tuning curves can be interpreted as a characteristic of functional lamination: single-peaked FRAs are representative of a spectrally uniform group of neurons within a functional lamina; double-peaked FRAs correspond to locations recording from neurons of two adjacent laminae. The fine spatial resolution necessary for defining a relationship between laminar and frequency organization, and the reconstruction of the frequency content of individual laminae, made it necessary to record activity from groups of neurons because it is not feasible consistently to isolate single neurons with the required spatial resolution. The same CFs and frequency steps were seen for advancing and retracting the electrode and for different electrode types.

A given 'frequency-band lamina' was reconstructed from the depth profile of several recording sites in three steps: (1) a CF plateau on a central penetration was chosen as the seed frequency for a functional lamina; (2) the horizontally closest penetration was selected and its CF plateau nearest to the seed frequency was determined, representing the most probable member of the same functional lamina as the seed frequency; (3) step 2 is repeated for the next nearest penetration until all penetrations have been included. Alignment for one lamina automatically defines the frequency content for all neighbouring laminae. In principle, the result of the alignment process does not depend on the initial seed frequency or penetration location.

Received 10 December 1996; accepted 2 May 1997.

1. Fletcher, H. Auditory patterns. *Rev. Mod. Physiol.* **12**, 47–65 (1940).
2. Zwicker, E. et al. Critical bandwidth in loudness summation. *J. Acoust. Soc. Am.* **29**, 548–557 (1957).
3. Greenwood, D. D. Critical bandwidth and the frequency coordinates of the basilar membrane. *J. Acoust. Soc. Am.* **33**, 1344–1356 (1961).
4. Watson, C. S. Masking of tones by noise for the cat. *J. Acoust. Soc. Am.* **62**, 167–172 (1963).
5. Yost, W. A. & Sheft, S. Across-critical band processing of amplitude modulated tones. *J. Acoust. Soc. Am.* **85**, 848–857 (1989).
6. Ehret, G. & Merzenich, M. M. Auditory midbrain responses parallel spectral integration phenomena. *Science* **227**, 1245–1247 (1985).
7. Ehret, G. & Merzenich, M. M. Complex sound analysis (frequency resolution filtering and spectral integration) by single units of the inferior colliculus of the cat. *Brain Res.* **13**, 139–163 (1988).
8. Pickles, J. O. Normal critical bands in the cat. *Acta Otolaryngol.* **80**, 245–254 (1975).
9. Pickles, J. O. & Comis, S. D. Auditory-nerve-fiber bandwidths and critical bandwidths in the cat. *J. Acoust. Soc. Am.* **60**, 1151–1156 (1976).
10. Ehret, G. Critical bands and filter characteristics in the ear of the house mouse (*Mus musculus*). *Biol. Cybern.* **24**, 35–42 (1976).
11. Ehret, G. & Moffat, A. J. M. Noise masking of tone responses and critical ratios of the mouse cochlear nerve and cochlear nucleus. *Hearing Res.* **14**, 45–57 (1984).
12. Pickles, J. O. Psychophysical frequency resolution in the cat as determined by simultaneous masking and its relation to auditory-nerve resolution. *J. Acoust. Soc. Am.* **66**, 1725–1732 (1979).
13. Evans, E. F. et al. Correspondence between behavioural and physiological frequency selectivity in the guinea pig. *Br. J. Audiol.* **23**, 151–152 (1989).
14. Nienhus, G. W. & Clark, G. M. Critical bands following the selective destruction of cochlear inner and outer haircells. *Acta Otolaryngol.* **88**, 350–358 (1979).
15. Suga, N. & Tsuzuki, K. Inhibition and level-tolerant frequency tuning in the auditory cortex of the mustached bat. *J. Neurophysiol.* **53**, 1109–1145 (1985).
16. Suga, N. Sharpening of frequency tuning by inhibition in the central auditory system: tribute to Yasuji Katsuki. *Neurosci. Res.* **21**, 287–299 (1995).
17. Merzenich, M. M. & Reid, M. D. Representation of the cochlea within the inferior colliculus of the cat. *Brain Res.* **77**, 397–415 (1974).
18. Roth, G. L. et al. Some features of the spatial organization of the central nucleus of the inferior colliculus of the cat. *J. Comp. Neurol.* **182**, 661–680 (1978).
19. Semple, M. N. & Aitkin, L. M. Representation of sound frequency and laterality by units in the central nucleus of the cat inferior colliculus. *J. Neurophysiol.* **42**, 1626–1639 (1979).
20. Rockel, A. J. & Jones, E. G. The neuronal organization of the inferior colliculus of the adult cat. I. The central nucleus. *J. Comp. Neurol.* **147**, 11–60 (1973).
21. Oliver, D. L. & Morest, D. K. The central nucleus of the inferior colliculus in the cat. *J. Comp. Neurol.* **222**, 237–264 (1984).
22. Oliver, D. L. Dorsal cochlear nucleus projections to the inferior colliculus in the cat: A light and electron microscope study. *J. Comp. Neurol.* **224**, 155–172 (1984).
23. Shneiderman, A. & Henkel, C. K. Banding of lateral superior olivary nucleus afferents in the inferior colliculus: a possible substrate for sensory integration. *J. Comp. Neurol.* **266**, 519–534 (1987).
24. Malmierca, M. S. et al. The central nucleus of the inferior colliculus in rat: A Golgi and computer reconstruction study of neuronal and laminar structure. *J. Comp. Neurol.* **333**, 1–27 (1993).
25. Chan, J. L. & Yin, T. C. T. Topographical relationships along the isofrequency laminae of the cat inferior colliculus: correlation with the anatomical lamination and representation of binaural response properties. *Soc. Neurosci. Abstr.* **8**, 348 (1982).
26. Schreiner, C. E. & Langner, G. Periodicity coding in the inferior colliculus of the cat. II. Topographical organization. *J. Neurophysiol.* **60**, 1823–1840 (1988).
27. Serviere, J. & Webster, W. R. A. A combined electrophysiological and [¹⁴C]-2-deoxyglucose study of the frequency organization of the inferior colliculus of the cat. *Neurosci. Lett.* **27**, 113–118 (1981).
28. Ehret, G. & Fischer, R. Neuronal activity and tonotopy in the auditory system visualized by c-fos gene expression. *Brain Res.* **567**, 350–354 (1991).
29. Pollak, G. D. & Park, T. J. The effects of GABAergic inhibition on monaural response properties of neurons in the mustache bat's inferior colliculus. *Hearing Res.* **65**, 99–117 (1993).
30. Palombi, P. S. & Caspary, D. M. GABA inputs control discharge rate primarily within frequency receptive fields of inferior colliculus neurons. *J. Neurophysiol.* **75**, 2211–2219 (1996).

Acknowledgements. Supported by the Office of Naval Research (C.E.S.) and the Deutsche Forschungsgemeinschaft (G.L.). We thank J. A. Winer for comments on the manuscript.

Correspondence and requests for materials should be addressed to C.E.S. (e-mail: chris@phy.ucsf.edu).

Kinesin hydrolyses one ATP per 8-nm step

Mark J. Schnitzer*† & Steven M. Block†‡

Departments of * Physics and † Molecular Biology, and ‡ Princeton Materials Institute, Princeton University, Princeton, New Jersey 08544, USA

Kinesin is a two-headed, ATP-dependent motor protein^{1,2} that moves along microtubules in discrete steps³ of 8 nm. *In vitro*, single molecules produce processive movement^{4,5}; motors typically take ~100 steps before releasing from a microtubule^{5–7}. A central question relates to mechanochemical coupling in this enzyme: how many molecules of ATP are consumed per step? For the actomyosin system, experimental approaches to this issue have generated considerable controversy^{8,9}. Here we take advantage of the processivity of kinesin to determine the coupling ratio without recourse to direct measurements of ATPase activity, which are subject to large experimental uncertainties^{8,10–12}. Beads carrying single molecules of kinesin moving on microtubules were tracked with high spatial and temporal resolution by interferometry^{3,13}. Statistical analysis of the intervals between steps at limiting ATP, and studies of fluctuations in motor speed as a function of ATP concentration^{14,15}, allow the coupling ratio to be determined. At near-zero load, kinesin molecules hydrolyse a single ATP molecule per 8-nm advance. This finding excludes various one-to-many and many-to-one coupling schemes, analogous to those advanced for myosin, and places severe constraints on models for movement.

Silica beads (0.5 μm diameter) were prepared with fewer than one molecule of kinesin, on average, bound nonspecifically to their surfaces. Beads were suspended in buffers containing variable amounts of ATP and introduced into a microscope flow cell. Individual diffusing beads were captured by an optical trap, deposited onto immobilized microtubules bound to the coverglass, and subsequent movements recorded with subnanometre resolution by optical-trapping interferometry^{3,13}. To ensure that beads were propelled by single molecules, they were prepared using extremely low concentrations of kinesin protein, sufficiently diluted from stock to make it unlikely that more than one molecule was present on a bead^{5,13}. In this regime, the fraction of beads moving as a function of kinesin concentration obeys Poisson statistics, confirming earlier findings^{4,5} (Fig. 1). To work at the lowest possible mechanical loads, the optical trap stiffness was set to just 7 fN nm⁻¹, producing a mean applied force of <0.9 pN in the optical trap (<15% of kinesin stall force¹³).

Average rates of kinesin movement were measured over three decades of ATP concentration. At saturating ATP levels, speeds were statistically identical to those measured by video tracking¹³ under no load, confirming the near-zero load condition. Speed data were well fit by Michaelis–Menten kinetics, with an apparent K_m for movement of $62 \pm 5 \mu\text{M}$ and k_{cat} of $680 \pm 31 \text{ nm s}^{-1}$, comparable to values found in microtubule gliding assays⁴ as well as solution studies of kinesin ATPase activity^{16–18}. This implies a Hill coefficient of one, and excludes models for movement that depart significantly from Michaelis–Menten kinetics¹⁹. Because hydrolysis activity in solution^{16–18} and speed *in vitro* display the same functional dependence on ATP, the coupling ratio—defined as the number of ATP molecules hydrolysed per mechanical advance—must be independent of ATP concentration. At limiting concentrations of ATP, k_{cat}/K_m gives a velocity of $11 \pm 1 \text{ nm s}^{-1} \mu\text{M}^{-1}$. In this regime, kinesin molecules advanced in clear increments of 8 nm (Fig. 2a), implying a stepping rate of $1.4 \pm 0.1 \mu\text{M}^{-1} \text{ s}^{-1}$ (Fig. 1). Statistical analysis of records, based on power spectra derived from pairwise distance differences⁵, revealed no signals corresponding to steps of

another size, although a small minority of steps of other sizes cannot be excluded (Fig. 2b,c). However, we did not confirm data from one study reporting roughly comparable numbers of 3-, 5- and 8-nm steps (ref. 20).

How long are the intervals between steps? Knowledge of this distribution at rate-limiting ATP may be used to determine the coupling. If kinesin molecules require just one ATP molecule per step, the distribution will be exponential, reflecting a solitary, rate-limiting biochemical reaction (binding of ATP). Conversely, a requirement for several (n) ATP molecules would lead to a distribution that is the convolution of n exponentials¹⁵. Pooling data from runs at 0.75, 1 and 2 μM ATP, during which steps could be identified in the records (Fig. 2), produced a distribution that was well fit by a single exponential (reduced $\chi^2 = 0.6$) with a rate of $1.1 \pm 0.1 \mu\text{M}^{-1} \text{s}^{-1}$ (Fig. 3a). This rate is in satisfactory agreement with the value derived independently from speed measurements (Fig. 1). In contrast, a convolution of two exponentials did not fit the data as well ($\chi^2 = 1.4$, $P(F = \chi^2_1/\chi^2_2) < 0.22$), and yielded a stepping rate ($0.8 \pm 0.06 \mu\text{M}^{-1} \text{s}^{-1}$) less compatible with k_{cat}/K_m . The observed step distribution supports the view that kinesin proteins bind a single ATP molecule before advancing by 8 nm.

To extend and confirm this finding, but without the need to identify individual stepwise transitions, we performed a fluctuation analysis of kinesin movement. For single processive motors, fluctuations about the average speed reflect the underlying enzyme stochasticity^{14,15}. Fluctuation analysis has been applied successfully to studies of the bacterial rotary motor²¹. Earlier work has shown that fluctuations can reveal the number of rate-limiting biochemical transitions per mechanical step^{14,15}; for kinesin molecules moving at saturating levels of ATP, there are approximately two such rate-limiting events¹⁴.

Fluctuation analysis of processive motor proteins relies on the determination of the randomness parameter, r , a dimensionless measure of the temporal irregularity between steps^{14,15}. A motor with $r = 0$ is perfectly clock-like, and takes an invariant time between steps. Conversely, a 'Poisson motor' with a single rate-limiting transition has $r = 1$. Additional rate-limiting transitions generally lead to $0 < r < 1$. For motors that step by a distance, d , whose positions are functions of time, $x(t)$, the randomness

parameter is defined as

$$r = \lim_{t \rightarrow \infty} \frac{\langle x^2(t) \rangle - \langle x(t) \rangle^2}{d \langle x(t) \rangle}, \quad (1)$$

where angle brackets denote the ensemble average. Both numerator and denominator in eqn (1) increase linearly with time (Fig. 2d), and their ratio approaches a constant whose reciprocal, r^{-1} , supplies a continuous measure of the number of rate-limiting transitions per step. Computations of the randomness parameter are robust to sources of thermal and instrumentation noise^{14,15}, thereby avoiding known difficulties associated with identifying individual steps against noisy backgrounds²². Nevertheless, the randomness parameter can be affected by factors that increase variance at long time scales, such as occasional backward steps, inactivated states, or steps of larger than normal size, which can all raise r beyond unity.

To ensure accurate determination of r , controls used both real and simulated data. We simulated runs at both saturating and limiting ATP conditions by generating stochastic 'staircase' records, consisting of 8-nm steps at either high or low average speeds ($\sim 630 \text{ nm s}^{-1}$, $\sim 10 \text{ nm s}^{-1}$) corrupted by gaussian white noise with total power comparable to that of real thermal noise. The times between steps were described by either an exponential distribution or a convolution of two exponentials. Fluctuation analysis of such records demonstrated

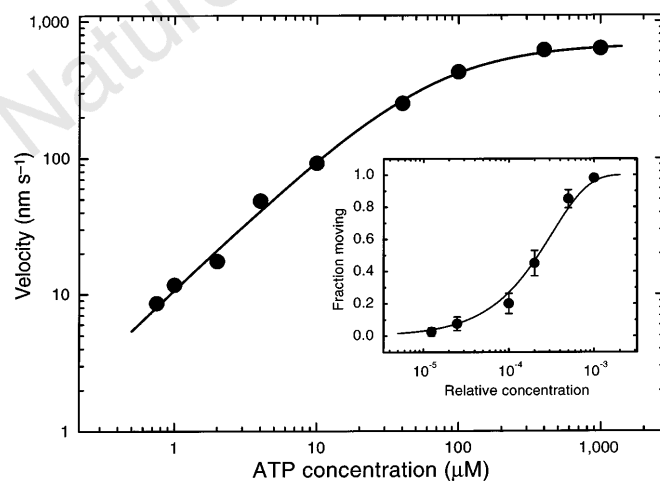


Figure 1 Average bead velocity, v , versus ATP concentration (double logarithmic plot). Error bars are smaller than data points (solid dots); each represents an average of 24–97 runs. Data fit to Michaelis-Menten kinetics (solid line), $v = k_{\text{cat}}[\text{ATP}]/(K_m + [\text{ATP}])$; $k_{\text{cat}} = 680 \pm 31 \text{ nm s}^{-1}$; apparent $K_m = 62 \pm 5 \mu\text{M}$. Inset, fraction of beads that moved, f , versus concentration of kinesin protein relative to stock, C (semilogarithmic plot). Values are expressed as mean \pm $\sqrt{f(1-f)/N}$. The one-parameter (λ) fit to Poisson statistics, $f = 1 - \exp(-\lambda C)$, (solid line, reduced $\chi^2 = 0.7$) confirms that single molecules suffice to move beads.

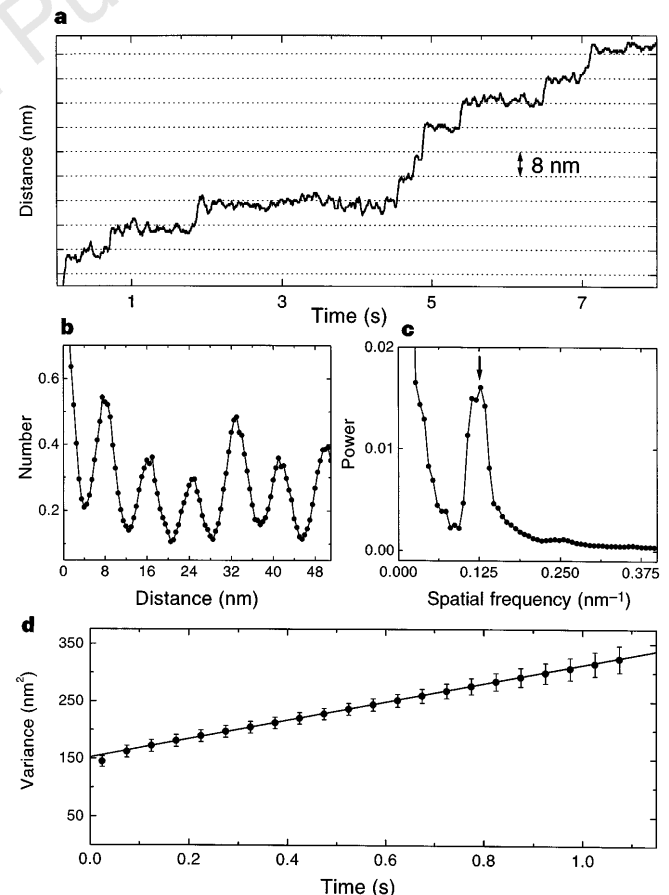


Figure 2 a, Sample record of movement at 2 μM ATP, showing the elementary steps (solid line). Horizontal grid lines (dotted lines) are spaced 8 nm apart. Data were median-filtered with a window width of 60 ms. **b**, Normalized histogram of pairwise distances between all pairs of data points in this record, showing a clear 8-nm periodicity. **c**, Normalized power spectrum of the data in **b**, displaying a single prominent peak at the reciprocal of 8 nm (arrow). **d**, Variance in position, averaged over 28 runs at 2 μM ATP (dots), and line fit over the interval 3.5 ms to 1.1 s. The y-intercept of the fit is determined by equipartition, $\langle x^2 \rangle = kT/\alpha$, where α is the combined stiffness of the optical trap and bead-microtubule linkage. The rapid rise in variance at short times reflects the brownian correlation time for bead position.

that r could be determined to better than 15%, and that the appropriate stepping statistics could thereby be distinguished (Table 1). To mimic data at low ATP, we fixed kinesin-coated beads on microtubules using 2 mM AMP-PNP, a non-hydrolysable ATP analogue. The microscope stage was then moved in nanometre-sized increments to generate simulated records with average speeds comparable to those in 1 μ M ATP (~ 10 nm s⁻¹) (Fig. 1). Once again, the number of rate-limiting transitions per step could readily be distinguished from the value of r . Individual steps in the latter records could also be detected by low-pass filtering the data. As a final control, we reconstructed interval distributions from these records; these were consistently fit by the appropriate model with either one or two rate-limiting steps (data not shown).

From records of kinesin-driven movement, we computed r as a function of ATP over a thousandfold range of concentration (Fig. 3). The qualitative shape of this relation had been predicted from the catalytic pathway^{14,15}. At high ATP levels, the curve is asymptotic to $r \approx \frac{1}{2}$. At intermediate ATP levels, the curve dips slightly, then rises at limiting ATP to a value near unity. The experimental value at saturating ATP confirms an earlier measurement¹⁴ and implies that each step involves a minimum of two rate-limiting transitions. Biochemical pathways derived from transient and steady-state kinetic studies also predict $r \approx \frac{1}{2}$ at high ATP levels, with the additional assumption that each mechanical step corresponds to one hydrolysis^{15,17,18}. For ATP levels near K_m , r drops as the rate of binding becomes comparably slow to other reactions. At limiting ATP, r rises through 1, reflecting a single rate-limiting transition occurring once per advance (ATP binding). The slight increase of r beyond unity reflects additional aspects of motor behaviour that tend to increase the variance.

Fluctuation analysis is robust to heterogeneity in the ATP binding rate (yielding heterogeneous mean speeds at limiting ATP), and controls allowed us to eliminate heterogeneity in bead size or in the stiffness of the bead–kinesin linkage as possible sources of additional variance (Table 1; Methods). Futile hydrolysis events that do not lead to a step can increase r , but not above unity¹⁴. Occasional pauses in movement, perhaps resulting from momentary sticking of beads to the coverglass or from motors transiently entering non-motile biochemical states, also increase variance. Sticking can be eliminated as an explanation because it would produce a concomitant reduction in brownian noise, and this was not observed. Transient inactive states causing $r \geq 1$ at limiting ATP result in even further increases beyond this value of randomness at moderate to saturating levels of ATP, and are therefore inconsistent with the

data. Two more possibilities merit examination: that ATP hydrolysis might occasionally produce backwards movement, a behaviour noted previously at higher external loads¹³ and also in this study; and that a single ATP hydrolysis might occasionally produce a double step of 16 nm, a transition that would appear indistinguishable from two 8-nm steps in rapid succession.

How frequent must such events be to give $r = 1.2$ – 1.5 at limiting ATP? We addressed this question by using analytical expressions for r subject to each of the candidate mechanisms (Methods). The observed randomness could be generated if either $\sim 16\%$ of steps were 16 nm or $\sim 7\%$ of steps were backwards. By visual examination of records, we scored 6–9% of all steps at low ATP as being backwards. However, using the identical approach, 4–5% of steps were spuriously identified as backwards in controls in which beads were attached in rigor and the stage stepped stochastically in one direction only. Neither mechanism (nor admixtures of the two) can therefore be eliminated, and either produces an acceptable, one-parameter fit to the data (Fig. 3b). However, the additional variance derives from a minority of events: 84–93% of 8-nm steps correspond to a single ATP hydrolysis. In contrast, if 16-nm steps per hydrolysis were the norm, this behaviour would be unmistakable in the records, and the value of r would be 2 (or more) at limiting ATP. Our data are equally incompatible with 8-nm steps arising from the hydrolysis of two ATP molecules, because neither mechanism is adequate to raise the limiting value of r at low ATP from 0.5 to the observed value: to do so would require that we fail to detect that in excess of $\sim 20\%$ of steps went backwards, and no fraction whatsoever of 16-nm advances alone could raise r from 0.5 to beyond 1.

These findings place important constraints on theories of kinesin movement. The Michaelis–Menten dependence of kinesin velocity⁴ (Fig. 1) is consistent with a solitary ATP binding event per step, and is incompatible with a simultaneous requirement for two ATP molecules. However, Michaelis–Menten kinetics are equally consistent with kinetic schemes in which two ATP molecules bind sequentially to each of two heads. This can happen, in particular, whenever the two binding events are separated by a kinetically irreversible transition. Specific examples include ATP binding to each of two cooperative sites in an ordered sequence to produce a step, or ATP binding irreversibly in random order to each of two non-interacting sites. Such possibilities are excluded by our data. Furthermore, we can exclude models in which kinesin molecules hydrolyse multiple ATPs per 8-nm step²³, and all models in which ATP hydrolysis results in an average advance in excess of 8–9 nm, (the so-called ‘many-to-one’ coupling scenarios^{9,11}). Models that remain consistent with our study include those in which the centroid of the molecule advances in increments of 8 nm (refs 22, 24, 25), for example through alternating 16-nm steps by each of the two heads^{23,26,27}, or those in which each ATP molecule produces a composite of two shorter ‘substeps’²⁸. However, to be consistent with our findings, substeps must obey certain constraints. First, one of the substeps must be ATP-dependent, whereas the other must be ATP-independent. Second, the ATP-independent substep must be at least as fast as k_{cat} (or faster), in view of the behaviour at saturating ATP levels. Putting in numbers, this implies the maximum duration between substeps must be under ~ 15 ms at low loads, and so could not be resolved with instrumentation such as ours. If substeps were somehow to be detected under other conditions (for example, if 8-nm steps were actually a composite of 3- and 5-nm substeps that could be visualized at moderate load, separated by ~ 50 ms and more²⁰) this would imply that the ATP-independent substep was strongly load dependent, and that its rate slowed dramatically with increased load. However, one model that incorporates substeps predicts that the second substep should proceed rapidly, not slowly, under such loads²³. Addressing this issue experimentally will require additional work at higher forces.

The size of the kinesin motor domain²⁹ is quite small, $4.5 \times 4.5 \times 7.0$ nm. A sequence of ~ 40 amino acids beyond the

Table 1 Controls in velocity and randomness determination

Number of runs	Step size (nm)	Transitions per step	Nominal velocity (nm s ⁻¹)	Velocity (nm s ⁻¹)	Nominal r	r
Computer						
80	8	1	630	642 ± 16	1	1.12 ± 0.03
80	8	2	630	638 ± 4	0.5	0.54 ± 0.01
30	8	1	8	8.6 ± 0.5	1	1.02 ± 0.16
30	8	2	8	8.4 ± 0.2	0.5	0.49 ± 0.05
30	4	1	8	7.7 ± 0.3	1	1.01 ± 0.09
Stage						
25	8.6 ± 0.1	1	8.6 ± 0.1	9.0 ± 0.6	1	0.88 ± 0.09
23	5.1 ± 0.1	1	10.2 ± 0.2	9.8 ± 0.3	1	0.88 ± 0.09
27	9.4 ± 0.2	2	9.4 ± 0.2	9.5 ± 0.3	0.5	0.54 ± 0.07
30	4.8 ± 0.2	2	9.6 ± 0.4	9.8 ± 0.3	0.5	0.58 ± 0.06

Controls for determination of velocity and randomness parameter, expressed as mean ± s.e.m. Computer-generated simulations of displacement records were used to test analysis procedures at both fast and slow speeds, corresponding to saturating and limiting ATP concentrations, respectively. At slow speeds, physical controls were performed using kinesin-coated beads fixed to microtubules by AMP-PNP. To simulate movement, the position of the piezoelectric microscope stage was displaced stochastically in discrete increments, separated by time intervals picked at random from either an exponential distribution or a convolution of two exponentials, under computer control. The size of steps was determined separately, using beads stuck directly to the coverglass, thereby removing the dominant source of brownian noise in position measurement. In every case, experimental and nominal values were in satisfactory agreement, and the value of r returned by this analysis distinguished unambiguously between one or two transitions per step.

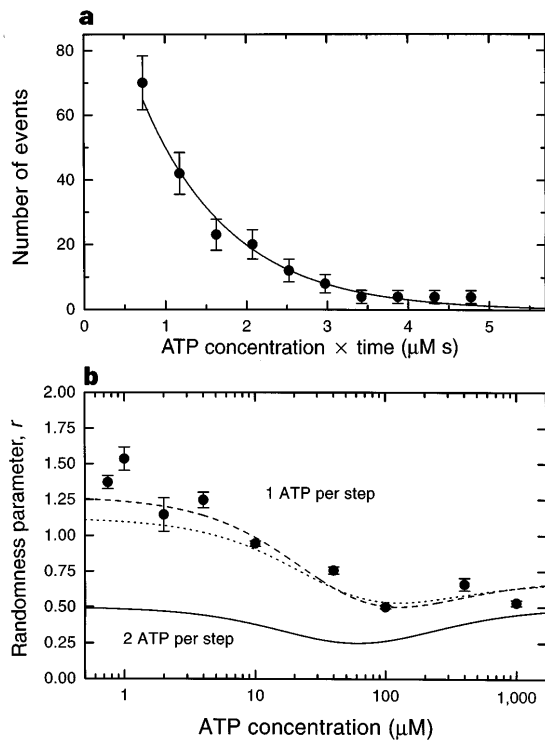


Figure 3 a, Histogram of times between steps for records at limiting ATP concentration (0.75, 1 and 2 μM). Data were pooled by weighting times by the ATP concentration. Values are expressed as $N \pm \sqrt{N}$. They fit to an exponential distribution (line) with a stepping rate of $1.1 \pm 0.1 \mu\text{M}^{-1} \text{s}^{-1}$ (reduced $\chi^2 = 0.6$). **b**, Semilogarithmic plot of the randomness parameter, r , versus ATP concentration. Experimental data (dots) and associated errors (s.e.m., based on 24–97 runs per determination) are compared to various models. Computed value of r , based on the k_{cat} and K_m values from Fig. 1, assuming two rate-limiting biochemical transitions at saturating ATP concentrations and two hydrolyses per step (solid line). There are no free parameters. Computed one-parameter (P_-) fit for r , based on the assumption of two rate-limiting biochemical transitions at saturating ATP concentrations and a single ATP hydrolysis per step, plus $P_- = 7\%$ backwards steps (dotted line). Computed one-parameter fit for r , based on the same assumptions, plus $P_{16} = 16\%$ of 16-nm steps (dashed line).

carboxy end of the crystal structure is thought to form an α -helix, and may supply an additional ~ 3 nm of leeway before the two kinesin heavy chains joint to form a coiled-coil tail. However, this segment is probably too short to constitute a ‘lever arm’ analogous to the structure proposed to be the site of displacement and force generation in myosin³⁰. An 8-nm step therefore poses challenges for understanding the molecular basis of kinesin movement. We anticipate that further applications of fluctuation analysis will supply useful clues to unravelling the mechanochemistry. Moreover, the power of this approach to provide insight into single-molecule kinetics makes it applicable to other processive systems, such as nucleic acid enzymes, including polymerases, helicases, topoisomerases and ribosomes. □

Methods

Assays. Motility assays were performed as previously described^{3,5,13}, except that microtubules were made from bovine brain tubulin (Cytoskeleton), coverslips were coated with poly-L-lysine rather than silanized, KCl was replaced by K-acetate, and an oxygen scavenging system (250 $\mu\text{g ml}^{-1}$ glucose oxidase, 30 $\mu\text{g ml}^{-1}$ catalase, 4.5 mg ml^{-1} glucose; Sigma) was used. An ATP regenerating system stabilized low ATP levels^{5,13}. Kinesin was purified from squid optic lobe as described¹. As a precaution against variability and to ensure work in the single molecule regime, only data from assays in which fewer than half of all beads moved were analysed.

Calibration and analysis. Optical-trapping interferometry and calibrations were performed as described^{3,13}. A trap stiffness of 7 fN nm^{-1} (average load $< 0.9 \text{ pN}$ over 50–200 nm from the trap centre) was obtained using 12 mW illumination at the specimen plane from a Nd:YLF laser (1047 nm, Spectra Physics). Interferometer output signals were sampled at 2 kHz, anti-alias filtered at 1 kHz, digitized at 12 bits, and stored by computer. Analysis programs were written in LabView 4.01 (National Instruments). Velocities, fluctuations and pairwise distances were analysed as described previously^{3,14}. Multiple runs over 50–200 nm from the trap centre were corrected to adjust for the kinesin-to-bead linkage compliance^{3,13}, except for the example in Fig. 2a, which was selected for low noise³. Mean velocities at each ATP concentration, $\langle v \rangle = \langle x(t) \rangle / t$, were determined by line fits to the average pairwise separation versus time for each run; slopes from such fits were averaged over all runs. The variance, $\langle x^2(t) \rangle - \langle x(t) \rangle^2$, was computed as the mean-squared deviation from the trajectory $\langle x(t) \rangle = \langle v \rangle t$, time-averaged for each run, then averaged over all runs. A line fit was made to this variance over the first 20 nm/ $\langle v \rangle$ time interval, after excluding the first 3.5 ms, because of the ~ 1 –3 ms correlation time for bead position^{3,14}. Theory and simulations show that a linear increase of variance with time (Fig. 2d) reflects a lack of any significant heterogeneity in mean velocity. The latter would produce a variance that grew quadratically with time. The standard error in variance also grew linearly with time, thereby supplying an error estimate for the slope. Randomness, r , was computed from the slope of the variance line fit divided by $d\langle v \rangle$. Experimental and control runs at limiting ATP levels were smoothed over a 5-ms time window with a linear filter, then decimated at 5-ms intervals, a procedure that reduces computation time but does not affect r . Subject to the minimal assumption of exactly two rate-limiting transitions per step at saturating ATP, r as a function of ATP concentration is determined by two parameters: the apparent Michaelis–Menten constant, and the ATP binding rate, determined in Fig. 1. To ascertain the effect of backward movements or 16-nm steps on r , we used the following expressions: $r = 1/(1 - 2P_-) + (\bar{r} - 1)/(1 - 2P_-)$, and $r = (1 + 3P_{16})/(1 + P_{16}) + (\bar{r} - 1)/(1 + P_{16})$, where P_- and P_{16} are the probabilities of backwards and 16-nm events, respectively, and \bar{r} is the randomness in their absence (M.J.S. and S.M.B., unpublished). By using experimental values for K_m and binding rate, the randomness data of Fig. 3 were fit to each of these expressions using a single free parameter. For analysis of pairwise distances and times between advances, runs at 0.75, 1 and 2 μM ATP were median-filtered with a window of 20–75 ms. Step times were identified by eye using custom software that returned the interval selected by cursors superposed on a graphical display of displacement versus time. Events shorter than 0.5 $\mu\text{M s}$ were excluded from analysis to avoid artefacts arising from the missing-event problem¹⁴.

Received 13 February; accepted 12 May 1997.

- Vale, R. D., Reese, T. S. & Sheetz, M. P. Identification of a novel force-generating enzyme, kinesin, involved in microtubule-based motility. *Cell* **42**, 39–50 (1985).
- Kreis, T. & Vale, R. D. *Guidebook to the Cytoskeletal and Motor Proteins* (Oxford Univ. Press, 1993).
- Svoboda, K., Schmidt, C. F., Schnapp, B. J. & Block, S. M. Direct observation of kinesin stepping by optical trapping interferometry. *Nature* **365**, 721–727 (1993).
- Howard, J., Hudspeth, A. J. & Vale, R. D. Movement of microtubules by single kinesin molecules. *Nature* **342**, 154–158 (1989).
- Block, S. M., Goldstein, L. S. B. & Schnapp, B. J. Bead movement by single kinesin molecules studied with optical tweezers. *Nature* **348**, 348–352 (1990).
- Vale, R. D. *et al.* Direct observation of single kinesin molecules moving along microtubules. *Nature* **380**, 451–453 (1996).
- Hackney, D. D. Highly processive microtubule-stimulated ATP hydrolysis by dimeric kinesin head domains. *Nature* **377**, 448–450 (1995).
- Burton, K. Myosin step size: estimates from motility assays and shortening muscle. *J. Muscle Res. Cell Motil.* **13**, 590–607 (1992).
- Yanagida, T., Harada, Y. & Ishijima, A. Nano-manipulation of actomyosin molecular motors *in vitro*: a new working principle. *Trends Biochem. Sci.* **18**, 319–324 (1993).
- Sowerby, A. J., Sehara, C. K., Lee, M. & Bagshaw, C. R. Turnover of fluorescent nucleoside triphosphates by isolated immobilized myosin filaments: transient kinetics on the septomole scale. *J. Mol. Biol.* **234**, 114–123 (1993).
- Harada, Y., Sakurada, K., Aoki, T., Thomas, D. D. & Yanagida, T. Mechanochemical coupling in actomyosin energy transduction studied by *in vitro* movement assay. *J. Mol. Biol.* **216**, 49–68 (1990).
- Toyoshima, Y. Y., Kron, S. J. & Spudis, J. A. The myosin step size: measurement of the unit displacement per ATP hydrolyzed in an *in vitro* assay. *Proc. Natl. Acad. Sci. USA* **87**, 7130–7134 (1990).
- Svoboda, K. & Block, S. M. Force and velocity measured for single kinesin molecules. *Cell* **77**, 773–784 (1994).
- Svoboda, K., Mitra, P. P. & Block, S. M. Fluctuation analysis of motor protein movement and single enzyme kinetics. *Proc. Natl. Acad. Sci. USA* **91**, 11782–11786 (1994).
- Schnitzer, M. J. & Block, S. M. Statistical kinetics of processive enzymes. *Cold Spring Harb. Symp. Quant. Biol.* **60**, 793–802 (1995).
- Hackney, D. D. The rate-limiting step in microtubule-stimulated ATP hydrolysis by dimeric kinesin head domains occurs while bound to the microtubule. *J. Biol. Chem.* **269**, 16508–16511 (1994).

17. Gilbert, S. P., Webb, M. R., Brune, M. & Johnson, K. A. Pathway of processive ATP hydrolysis by kinesin. *Nature* **373**, 671–676 (1995).
18. Ma, Y. & Taylor, E. W. Kinetic mechanism of the kinesin motor domain. *Biochemistry* **34**, 13242–13251 (1995).
19. Leibler, S. & Huse, D. A. Porters versus rowers: a unified stochastic model of motor proteins. *J. Cell Biol.* **121**, 1357–1368 (1993).
20. Coppin, C. M., Finer, J. T., Spudis, J. A. & Vale, R. D. Detection of sub-8-nm movements of kinesin by high-resolution optical-trap microscopy. *Proc. Natl Acad. Sci. USA* **93**, 1913–1917 (1996).
21. Samuel, A. D. T. & Berg, H. C. Torque-generating units of bacterial flagellar motor step independently. *Biophys. J.* **71**, 918–923 (1996).
22. Block, S. M. & Svoboda, K. Analysis of high resolution recordings of motor movement. *Biophys. J.* **68**, 230s–241s (1995).
23. Duke, T. & Leibler, S. Motor protein mechanics: a stochastic model with minimal mechanochemical coupling. *Biophys. J.* **71**, 1235–1247 (1996).
24. Hackney, D. D. Evidence for alternating head catalysis by kinesin during microtubule-stimulated ATP hydrolysis. *Proc. Natl Acad. Sci. USA* **91**, 6865–6869 (1994).
25. Gelles, J. *et al.* Structural and functional features of one- and two-headed biotinylated kinesin derivatives. *Biophys. J.* **68**, 276s–282s (1995).
26. Howard, J. The movement of kinesin along microtubules. *Annu. Rev. Physiol.* **58**, 703–729 (1996).
27. Peskin, C. S. & Oster, G. Coordinated hydrolysis explains the mechanical behavior of kinesin. *Biophys. J.* **68**, 202s–211s (1995).
28. Derenyi, I. & Vicsek, T. The kinesin walk: a dynamic model with elastically coupled heads. *Proc. Natl Acad. Sci. USA* **93**, 6775–6779 (1996).
29. Kull, F. J., Sablin, E. P., Lau, R., Fletterick, R. J. & Vale, R. D. Crystal structure of the kinesin motor domain reveals a structural similarity to myosin. *Nature* **380**, 550–555 (1996).
30. Block, S. M. Fifty ways to love your lever: myosin motors. *Cell* **87**, 151–157 (1996).

Acknowledgements. We thank S. Gross, W. Ryu, L. Satterwhite, M. Wang and especially K. Visscher for technical assistance and discussions; S. Gross for help in purifying kinesin; and P. Mitra and K. Svoboda for advice in the early stages of this project. This work was supported by a grant from NIGMS (S.M.B.) and predoctoral fellowships from NSF and American Heart Association (M.J.S.).

Correspondence should be addressed to M.J.S. (e-mail: schnitzr@princeton.edu).

Coupling of kinesin steps to ATP hydrolysis

Wei Hua*, Edgar C. Young, Margaret L. Fleming & Jeff Gelles

* *Biophysics and Structural Biology Graduate Program, Department of Biochemistry, and The Center for Complex Systems, Brandeis University, Waltham, Massachusetts 02254, USA*

A key goal in the study of the function of ATP-driven motor enzymes is to quantify the movement produced from consumption of one ATP molecule^{1–3}. Discrete displacements of the processive motor kinesin along a microtubule have been reported as 5 and/or 8 nm (refs 4, 5). However, analysis of nanometre-scale movements is hindered by superimposed brownian motion. Moreover, because kinesin is processive and turns over stochastically, some observed displacements must arise from summation of smaller movements that are too closely spaced in time to be resolved. To address both of these problems, we used light microscopy instrumentation⁶ with low positional drift (< 39 pm s⁻¹) to observe single molecules of a kinesin derivative moving slowly (~2.5 nm s⁻¹) at very low (150 nM) ATP concentration, so that ATP-induced displacements were widely spaced in time. This allowed increased time-averaging to suppress brownian noise (without application of external force^{4,5}), permitting objective measurement of the distribution of all observed displacement sizes. The distribution was analysed with a statistics-based method which explicitly takes into account the occurrence of unresolved movements, and determines both the underlying step size and the coupling of steps to ATP hydrolytic events. Our data support a fundamental enzymatic cycle for kinesin in which hydrolysis of a single ATP molecule is coupled to a step distance of the microtubule protofilament lattice spacing of 8.12 nm (ref. 7). Step distances other than 8 nm are excluded, as is the coupling of each step to two or more consecutive ATP hydrolysis reactions with similar rates, or the coupling of two 8-nm steps to a single hydrolysis. The measured ratio of ATP consumption rate to stepping rate is invariant over a wide range of ATP concentration, suggesting that the 1 ATP to 8 nm coupling inferred from behaviour at low ATP can be generalized to high ATP.

Box 1 Distribution of displacements observed with limited time resolution

Detection of processive motor steps can be modelled analytically. We assume that, in the absence of noise, every displacement detected has size nd_1 , where n is a positive integer and d_1 is the unitary step size. We model the effects of a step discrimination method in which the time interval t between neighbouring unitary steps is detected only if $t >$ the time resolution, t_r . In this case, the probability that $n = 1$ is

$$P_1 = P(t > t_r),$$

where $P(t > t_r)$ is the probability that the interval $t > t_r$. The probability that $n = 2$ is the probability of not detecting the interval between one pair of unitary steps and detecting the interval between the next pair:

$$P_2 = [1 - P(t > t_r)]P(t > t_r) = (1 - P_1)P_1.$$

In general,

$$P_n = P_1(1 - P_1)^{n-1}.$$

The histogram of observed displacements will be:

$$H(x) = N' \begin{cases} P_n & x = nd_1 \text{ with } n = 1, 2, 3, \dots \\ 0 & \text{elsewhere,} \end{cases}$$

where N' is the total number of displacements detected. N' also corresponds to the maximum value in the cumulative histogram,

$$C(d) = \int_0^d H(y) dy.$$

$C(d)$ differs from the cumulative histograms shown in Fig. 3, in that the latter include effects of experimental noise (see Methods). The total number of unitary steps $\tilde{N} = D/d_1$, where D is the total distance moved, and

$$\tilde{N} = N' \sum_{i=1}^{\infty} iP_i = N'/P_1.$$

At limiting ATP concentrations, mechanisms with the same d_1 but different coupling of steps to ATP hydrolysis give different $P(t > t_r)$ and therefore different histograms. For example, for a mechanism in which each unitary step is coupled to the hydrolysis of one ATP molecule,

$$P(t > t_r) = e^{-t/\tau},$$

where $\tau = Td_1/D$ is the average time interval between steps, and T is the total time. In contrast, if each step is followed by two consecutive ATP hydrolysis events with rate constant ratio k ,

$$P(t > t_r) = \frac{e^{-[(k+1)t/\tau]} - k e^{-[k+1)t/\tau}}{1 - k}.$$

These results can be generalized to apply to mechanisms that include more than one unitary step size.

K448-BIO is a recombinant biotinylated protein containing the amino-terminal 448 amino acids of the *Drosophila* kinesin heavy chain (including the motor domain, which is sufficient for microtubule-based motility⁸). It forms stable dimers⁹ and so, like intact kinesin¹⁰, it contains two active sites. K448-BIO displays kinesin-like ATPase activity⁹, and single dimers of K448-BIO attached to streptavidin beads move processively^{11,12} (that is, for hundreds of nanometres without detaching from the microtubule), like intact kinesin^{13,14} and other dimeric kinesin derivatives¹⁵. The rate of forward translocation by single molecules displays hyperbolic dependence on ATP concentration (Fig. 1a). The fitted Michaelis–Menten parameters from velocities at ATP concentrations $\geq 5 \mu\text{M}$ are confirmed by the slope of the linear ATP dependence of velocities at sub-micromolar ATP levels (Fig. 1a, inset). This strict hyperbolic dependence is consistent with a reaction sequence in which the two active sites of the enzyme bind ATP in a sequential manner, provided that an irreversible step, such as phosphate release, occurs between the two binding reactions. (A mechanism without an intervening irreversible step has a non-hyperbolic rate law¹⁶.)

The ATP consumption associated with the motor's movement